International Journal of Nanoelectronics and Materials
IJNeaM
ISSN 1985-5761 | E-ISSN 2232-1535

Enhanced charge transport via Fe-doped brookite TiO_2 ETLs for eco-friendly perovskite solar cells

Rupesh Mahamune [a]*, Modugu Krishnaiah [b], Kapil Jajulwar [c], and Neerja S. Dharmale [a]

[a]*Department of Electronics and Telecommunication Engineering Shri Sant Gajanan Maharaj College of Engineering, Shegaon, Maharashtra 444203, India*
[b]*Dept. Electronics and Telecommunication engineering, Vidya Jyothi Institute of Technology, Rangareddy, Hyderabad-075, Telangana, India*
[c]*Department of Electronics and Communication Engineering G HRAISONI College of Engineering Nagpur, India*
∗Corresponding author. Tel.: +91-691-330-8391; e-mail: rupesh.mahamune@gmail.com

Received 09 May 2025, Revised 08 October 2025, Accepted 04 March 2026

ABSTRACT

Through detailed simulation studies, essential material properties—such as bandgap energy (E_g), dielectric constant (ε), effective density of states for both conduction (N_c) and valence (N_v) bands, and the thermal velocities of charge carriers (V_{the} for electrons and V_{thh} for holes)—were obtained via density functional theory (DFT) calculations. These properties served as inputs for Solar Cell Capacitance Simulator in 1 Dimension (SCAPS-1D) simulations to assess and enhance the efficiency of perovskite solar cells (PSCs) featuring Fe-doped brookite titanium dioxide (TiO_2) as the electron transport layer (ETL). The study involved optimizing both the absorber and ETL to achieve improved charge transport and overall efficiency. Key device metrics, including current-voltage (JV) curves and quantum efficiency (QE) were thoroughly examined. Simulation outcomes indicate that Fe doping significantly boosts the electron transport properties of brookite TiO_2, leading to better interface characteristics and enhanced charge carrier mobility. The optimized device demonstrated a remarkable power conversion efficiency (PCE) of 31.40%, underscoring the promise of Fe-doped brookite TiO_2 as a stable, efficient, and environmentally friendly ETL material for next-generation lead-free perovskite solar cell (PSC). This study highlights the value of integrating first-principles calculations with device-level modeling to drive innovation in solar energy technologies.

Keywords: *DFT, Lead free-perovskite solar cell (PSC), SCAPS-1D simulation, Electron transport layer (ETL), Brookite phase of TiO_2, Defect*

1. INTRODUCTION

Current research on perovskite solar cells (PSCs) is primarily focused on enhancing their efficiency, operational stability, and environmental sustainability. Although lead-based perovskites such as methylammonium lead halide ($CH_3NH_3PbI_3$) have demonstrated outstanding photovoltaic performance, issues related to toxicity and poor long-term stability have shifted research toward lead-free perovskite alternatives [1]. In these devices, the electron transport layer (ETL) plays a pivotal role in charge extraction, transport, and recombination suppression, thereby influencing overall device efficiency and lifetime [2].

Among various ETL materials, titanium dioxide (TiO_2) has been extensively utilized due to its suitable band alignment, excellent chemical stability, and low cost [3]. However, pristine TiO_2 suffers from several inherent limitations, including high electron–hole recombination rates, low conductivity, and poor light absorption, which restrict its performance in PSCs [4]. Moreover, the presence of surface defects in undoped TiO_2 can act as recombination centres, further degrading charge transport efficiency [5]. These challenges are particularly significant in lead-free perovskite systems, where charge dynamics and band alignments differ markedly from their lead-based counterparts [6].

To overcome these drawbacks, doping TiO_2 with metal [7, 8] and non-metal elements has emerged as a promising approach to tune its structural, electrical, and optical properties [9]. Metal dopants such as zinc (Zn), niobium (Nb), and fluorine (F) have been reported to enhance electron mobility, surface passivation, and conductivity in the ETL, resulting in improved photovoltaic performance [10–14]. Similarly, non-metal dopants like nitrogen (N), carbon (C), and sulfur (S) effectively reduce the bandgap, suppress recombination losses, and increase visible-light absorption, thereby boosting charge transport efficiency in lead-free perovskite devices [15–17]. Co-doping strategies (e.g., N–F or iron (Fe)–S) have also been explored to achieve synergistic improvements in TiO_2 performance for thin-film solar cells [18, 19]. A planar perovskite solar cell (PSC) incorporating a Ta/Nb co-doped TiO_2 ETL demonstrates an enhanced power conversion efficiency of 19.44%, outperforming the pristine TiO_2-based device, which exhibits 17.60%. The outcomes of this study offer valuable perspectives on developing cost-effective and high-efficiency PSCs through low-temperature fabrication techniques [20].

Brookite-based ETLs have demonstrated superior photovoltaic performance relative to anatase in certain PSC configurations. [21, 22]. Bhandari *et al.* [23] explored brookite nanorods as ETL, achieving promising results

attributed to improved perovskite–ETL interfacial cohesion and enhanced open-circuit voltage (V_{OC}) compared to anatase-based reference cells. In reference [24], the authors investigated and compared the performance of single-phase anatase (A) and brookite (B), as well as heterophase combinations of anatase–brookite (AB) and brookite–anatase (BA), when used as ETLs in PSCs (PSCs). The PSC employing a low-temperature-processed single-layer fluorine-doped tin oxide (FTO)-B ETL achieved a power conversion efficiency (PCE) of 14.92%, representing the highest reported efficiency for a single-layer FTO-B-based PSC. These findings indicate that FTO-B functions as an active phase and holds strong potential as an n-type ETL scaffold for planar PSC architectures. Doping brookite TiO_2 plays a crucial role in enhancing the interfacial quality and electronic properties of PSCs. The introduction of dopant ions, such as Sc^{3+}, into the brookite TiO_2 lattice effectively reduces surface and bulk defects, leading to better charge transport and minimized carrier recombination. Moreover, doped brookite TiO_2 facilitates improved energy level alignment with the perovskite absorber, ensuring efficient electron extraction and enhanced device stability. As a result, PSCs employing doped brookite TiO_2 scaffolds exhibit higher power conversion efficiency and superior long-term stability compared to undoped counterparts [25].

Although significant progress has been made in developing brookite TiO_2 and its doped variants, the influence of transition metal dopants—particularly Fe—on tailoring the brookite phase of TiO_2 remains insufficiently investigated. Brookite TiO_2 inherently exhibits higher electron mobility and favourable energy level alignment with lead-free perovskites such as $CH_3NH_3SnI_3$, making it an attractive candidate for ETLs [26]. The incorporation of Fe into the brookite TiO_2 lattice can alter its electronic structure, suppress defect states, and improve charge carrier mobility through d-orbital hybridization effects [27]. Nevertheless, a comprehensive understanding of Fe-induced electronic and interfacial modifications and their subsequent influence on device performance remains limited due to the scarcity of experimental studies.

The research gap therefore lies in the lack of a systematic investigation into the relationship of Fe-doped brookite TiO_2 as an ETL for lead-free PSCs. This study bridges that gap by integrating DFT and SCAPS-1D simulations to analyse how Fe doping alters key electronic parameters—such as bandgap energy, density of states, and carrier transport characteristics—and how these modifications translate into enhanced photovoltaic performance.

In summary, this work introduces Fe-doped brookite TiO_2 as a novel, stable, and environmentally benign ETL material that can significantly improve charge transport and interfacial properties in lead-free PSCs. The findings provide critical insights for the design of next-generation non-toxic, high-efficiency perovskite photovoltaic devices.

2. PSC USING SCAPS-1D

A PSC with a glass/FTO/Fe-doped TiO_2/$CH_3NH_3SnI_3$/cuprous oxide (Cu_2O)/Gold (Au) structure is designed using the Solar Cell Capacitance Simulator in 1 Dimension (SCAPS-1D). The absorber layer is methylammonium tin iodide ($CH_3NH_3SnI_3$), FTO is the transparent conducting oxide (TCO), Cu_2O is used as hole transport layer (HTL), and the ETL is Fe-doped brookite TiO_2. Some of the layers simulation settings are collected from ref. [17–19, 26–31, 46]. These variables have been optimized and are listed in Table 1.

Doping ETL causes an increase in solar cell performance. According to the authors [32–34], doped TiO_2 instead of un-doped TiO_2 enhanced device performance because doping enables a configurable bandgap and Fermi level, which permits V_{OC} variation. Interface defect layer 1 (IDL_1) and Interface defect layer 2 (IDL_2) have been introduced as interface layers for $CH_3NH_3SnI_3/Cu_2O$ and $TiO_2/CH_3NH_3SnI_3$ interfaces, respectively, to make the device more practical. A portion of the charge carriers is trapped at the interface layers. A schematic for simulated solar cells is shown in Figure 1. ETL was made up of Fe-doped TiO_2.

Figure 1. Simulated PSC using Fe-doped brookite TiO_2 as ETL

3. OPTIMISING THICKNESS, SHALLOW DONAR DENSITY, AND DEFECTS OF ETL

When optimizing ETL parameters, factors such as thickness (t), shallow donor density (N_D), and the densities of two types of defects (N_{t1} and N_{t2}) are taken into account to improve efficiency. The range in which these parameters are varied is shown in Table 1. The optimized value for t, N_D, N_{t1} and N_{t2} are found to be 0.1 μm, 1×10^{22} cm^{-3}, 1×10^{17} cm^{-3}, and 1×10^{16} cm^{-3}. In this context, we observe two types of defects: a neural defect (N_{t1}) [35] and a single donor defect (N_{t2}) [36]. Increasing N_{t1} results in decreased mobility and minority carrier longevity, although it has minimal impact on cell characteristics. This finding is supported by the conclusions in reference [35]. Thus, we are examining these two specific defects in our analysis.

Table 1. Data used for SCAPS simulation

Parameters with its definition	ETL Fe-TiO_2	ID1	$CH_3NH_3SnI_3$	ID2	Cu_2O	FTO
T (μm): Thickness of the material layer, representing the physical depth of each functional layer (e.g., absorber, ETL, HTL) in micrometers, which directly influences light absorption and charge transport.	0.1-0.8	0.01	0.8–1.6	0.01	0.4	0.5 [17]
Eg (eV): Bandgap energy, denoting the energy difference between the valence band maximum and conduction band minimum; it determines the spectral absorption range of the material.	*1.58	1.31	1.3	1.3	2.17 [18]	3.5 [18]
χ (eV): Electron affinity, defined as the energy difference between the vacuum level and the conduction band minimum, governing electron transfer across interfaces.	3.9	4.17	4.17 [17]	4.17	3.2 [26]	4 [18]
ε: Relative dielectric constant (permittivity), indicating the material's ability to screen electric fields and reduce Coulombic interactions between charge carriers.	*6.76	8.2	8.2 [27]	8.2	7.1	9 [18]
N_C (cm^{-3}): Effective density of states in the conduction band, representing the number of available electronic states per unit volume for electrons.	$*3.3636 \times 10^{17}$	1×10^{18}	1×10^{18} [27]	1×10^{18}	2×10^{17}	1×10^{19}
N_V (cm^{-3}): Effective density of states in the valence band, representing the number of available energy states per unit volume for holes.	$*2.249 \times 10^{19}$	1×10^{18}	1×10^{18} [27]	1×10^{18}	1×10^{19}	1×10^{19}
V_{the} (cm/s): Thermal velocity of electrons, defining the average velocity of thermally excited electrons contributing to carrier transport.	$*4.914 \times 10^{7}$	1×10^{7}	1×10^{7}	1×10^{7}	1×10^{7} [18]	-
V_{thh} (cm/s): Thermal velocity of holes, describing the average speed of thermally generated holes within the semiconductor.	$*1.21 \times 10^{7}$	1×10^{7}	1×10^{7}	1×10^{7}	1×10^{7}	1×10^{7} [18]
μ_n ($cm^2/V{\cdot}s$): Electron mobility, indicating how quickly electrons move through the material under an applied electric field, affecting current transport and conductivity.	5 [46]	5 [46]	2×10^{3} [19]	2×10^{3}	2×10^{2}	1×10^{3}
μ_p ($cm^2/V{\cdot}s$): Hole mobility, defining the drift velocity of holes per unit electric field; crucial for efficient charge extraction.	5 [19]	3×10^{2}	3×10^{2} [27]	3×10^{2}	1×10^{1}	1×10^{1}
N_D (cm^{-3}): Donor concentration, referring to the density of donor dopants that supply free electrons in n-type semiconductor regions.	1×10^{22}	-	-	-	-	2×10^{18}
N_A (cm^{-3}): Acceptor concentration, referring to the density of acceptor dopants that introduce holes in p-type semiconductor regions.	-	1×10^{16}	1×10^{19}	1×10^{16}	1×10^{18}	-

Note: * represents values calculated using DFT.

4. OPTIMISING THICKNESS, SHALLOW ACCEPTOR DENSITY, AND DEFECT OF ABSORBER LAYER

Absorber layer parameters such as thickness(t), shallow acceptor density (N_A), and defect density (N_{t1}) are optimized with respect to efficiency value. The range in which these parameters are varied is shown in Table 1. The optimized value for t, N_A, N_{t1} are found to be 1.4 μm, 1×10^{18} cm^{-3}, and 1×10^{15} cm^{-3}. Flaws may appear on the absorber layer's surfaces as well as within the bulk. Perovskite-based absorber layers show several kinds of point defects, such as lattice vacancies, interstitials, and Frenkel defects [37]. Furthermore, defects like dislocations and grain boundaries exist. Impurities introduced through doping create shallow levels in the band gap [38–41]. These defects can trap charge carriers and enhance nonradiative electron-hole recombination [42–44]. Reference [27] discusses a neutral defect with a Gaussian distribution, which is considered here as well.

5. JV CHARACTERISTIC AND QUANTUM EFFICIENCY

Optimal current density–voltage characteristics (JV) is shown in Figure 2 (a). JV curve exhibits a sharp decline in current density (J_{sc}) near the open-circuit voltage ($V_{oc} \approx 1.05$ V), indicating efficient carrier extraction and minimal recombination losses within the device. The high short-circuit current density (~ 38 mA/cm^2) reflects excellent photon absorption and charge transport through the Fe-doped brookite TiO_2 ETL, confirming strong photovoltaic activity and good interface alignment with the perovskite absorber.

The quantum efficiency (QE) is seen in Figure 2 (b) and it is found that at $\lambda = 300$ nm, QE is 92.81%. The external quantum efficiency remains nearly constant ($\sim$ 95–100%) across a broad spectral range (350–850 nm), demonstrating effective light harvesting and minimal optical losses. The slight drop beyond 900 nm corresponds to the absorption edge of the perovskite layer, confirming optimal bandgap matching and efficient photo response throughout the visible region. This behaviour signifies superior carrier collection and low recombination, validating the material's suitability for high-efficiency PSC applications.

Table 2 represents J_{sc}, V_{oc}, FF, and η of the optimized cell, while Table 1 represents optimized cell parameters. A comparative evaluation of the present Fe-doped TiO_2-based PSC with previously reported architectures demonstrates a significant enhancement in device performance. The simulated PSC configuration of Glass/FTO/Fe-doped-TiO_2/$CH_3NH_3SnI_3$/Cu_2O/Au achieved a power conversion efficiency (PCE) of 31.40%, with J_{sc} of 34.56 mA/cm^2, V_{oc} of 1.0679 V, and a fill factor (FF) of 85.08%. This performance surpasses all experimentally reported devices, including pristine TiO_2-based PSCs ($\eta = 22.16\%$) and S-doped TiO_2 systems ($\eta = 23.58\%$) [1], as well as Sc^{3+}-doped brookite TiO_2-based devices ($\eta = 21.75\%$) [25].

The observed improvement can be attributed to the synergistic effects of Fe doping, which modify the electronic structure of TiO_2, reduce trap states, and enhance charge transport at the ETL–perovskite interface. Additionally, the simulated environment allows for idealized material interfaces and optimized charge carrier dynamics, leading to a higher theoretical efficiency compared to experimentally fabricated devices that often face losses due to surface roughness, non-uniform films, or interfacial defects.

Table 2. Simulated cell parameters in comparison with existing literature

PSC	J_{sc} (mA/cm^2)	V_{oc} (V)	FF (%)	η (%)
Glass/FTO/Fe-Doped-TiO_2/$CH_3NH_3SnI_3$/Cu_2O/A [This Work]	34.56	1.0679	85.08	31.40
Glass/FTO/P-TiO_2/$CH_3NH_3SnI_3$/Cu_2O/Au [1]	32.918	0.869	77.411	22.165
Glass/FTO/S-doped TiO_2/$CH_3NH_3SnI_3$/Cu_2O/Au [1]	25.923	1.062	85.54	23.583
*FTO/PEDOT:PSS/P3HT:S-doped TiO_2/Al [17]	3.18 ± 0.06	0.67 ± 0.05	0.44 ± 0.05	0.96 ± 0.1
*FTO/PEDOT:PSS/P3HT:P-TiO_2/Al [17]	2.37 ± 0.06	0.61 ± 0.05	0.42 ± 0.05	0.62 ± 0.1
*Un-doped [47]	20.02	1.022	71	14.46
*Glass/FTO/BL/TiO_2(Anatase/brookite/rutile)/ZrO_2 or Al_2O_3/carbon [48]	20–24	0.85–0.89	55–60	11
*Brookite TiO_2 (BTO) rod [23]	22.1	1062.5	64	15.02
*Brookite TiO_2 (BTO) cube [23]	21.42	1047.0	62.5	14.0
*Commercial TiO_2 [23]	21.14	1026.25	61.2	13.27
*FTO/SnO_2/brookite TiO_2(Sc^{3+} doped)/perovskite/Spiro-OMeTAD/Au [25]	-	-	-	21.75

Note: * indicates experimental work.

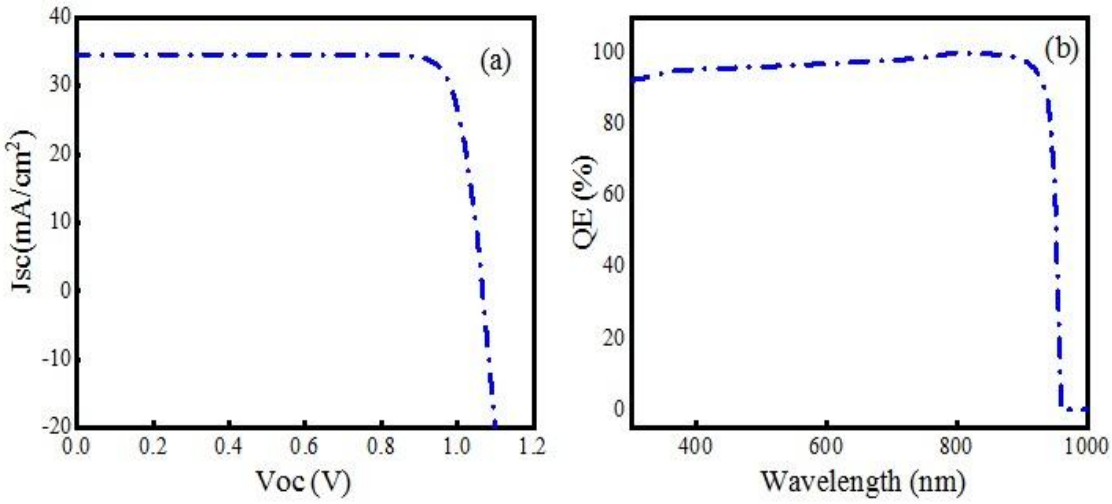

Figure 2. (a) J–V characteristics of the simulated device. (b) Quantum efficiency (QE) spectrum

Therefore, the superior simulated efficiency of 31.40% highlights the strong potential of Fe-doped brookite TiO_2 as an efficient ETL for future high-performance PSCs, providing a valuable theoretical benchmark for experimental optimization.

6. LIMITATIONS OF THE SIMULATION APPROACH

Fabrication of pure brookite TiO_2 remains challenging due to its metastable nature and strong tendency to transform into anatase or rutile. Its synthesis requires precise control of pH, temperature, precursor chemistry, and reaction conditions; even minor variations often yield mixed phases, limiting reproducibility and large-scale production [45].

While the integration of density functional theory (DFT) using Quantum ATK and SCAPS-1D simulations provides valuable insights into the electronic and photovoltaic behaviour of Fe-doped brookite TiO_2, several limitations must be acknowledged. DFT assumes ideal crystalline structures under equilibrium conditions, neglecting real-world imperfections such as grain boundaries, structural defects, and disorder that can strongly affect carrier transport and recombination dynamics.

Similarly, SCAPS-1D employs simplified drift–diffusion models that treat interfaces as perfectly abrupt and defect-free. In practical devices, interfacial traps, surface roughness, and chemical inhomogeneities between the perovskite absorber and the Fe-doped TiO_2 ETL introduce non-radiative recombination pathways, reducing carrier lifetime and open-circuit voltage. Furthermore, temperature effects, ion migration, and long-term degradation are not fully captured in the steady-state SCAPS framework, potentially leading to overestimated power conversion efficiencies (PCE).

Additionally, simulation parameters derived from DFT—such as bandgap, dielectric constant, and carrier mobility—represent intrinsic, idealized values. Experimental variations in stoichiometry, dopant distribution, and synthesis methods may cause significant deviations from these assumptions. Lastly, environmental influences including humidity, oxygen exposure, and operational aging are not considered in the current simulations, limiting their real-world applicability [23].

7. CONCLUSION

Doped TiO_2 has demonstrated great potential as an ETL for lead-free PSCs, offering improved charge transport, enhanced stability, and superior photovoltaic performance. In this study, Fe-doped TiO_2 achieved a simulated power conversion efficiency of 31.40%, highlighting its theoretical promise in optimizing interfacial charge dynamics and reducing recombination losses. However, this high efficiency is obtained under idealized simulation conditions that neglect real-world fabrication and environmental factors. Therefore, experimental validation is essential to confirm these results and to further translate the simulated advantages of doped TiO_2 into practical, stable, and scalable PSC devices.

8. FUTURE SCOPE

To advance the practical application of Fe-doped brookite TiO_2 as an ETL, future research should prioritize its experimental validation within carbon-based, fully printed PSCs (C-PSCs), which offer enhanced stability and cost efficiency. Detailed structural (X-ray diffraction (XRD), transmission electron microscopy (TEM)), optical (ultraviolet–visible spectroscopy (UV–Vis), photoluminescence (PL)), and electrical (electrochemical impedance spectroscopy (EIS), current density–voltage (JV) analyses will be crucial to substantiate the simulated findings and evaluate real-world performance. Additionally, combining these experiments with advanced computational techniques—such as non-equilibrium Green's function (NEGF) analysis and multidimensional SCAPS simulations—can yield deeper insights into interfacial charge dynamics, defect behaviour, and degradation pathways, thereby guiding the development of robust, lead-free, and high-efficiency PSCs.

REFERENCES

[1] N. Dharmale, A. Srivastava, and S. Chaudhury, "Performance analysis of un-doped and doped titania (TiO_2) as an electron transport layer (ETL) for perovskite solar cells," *Journal of Molecular Modeling*, vol. 30, no. 154, pp. 154, 2024.

[2] N. Dharmale, S. Chaudhury, and C. K. Pandey, "Theoretical investigation on un-doped and doped TiO_2 for solar cell application," *Physica Scripta*, vol. 97, no. 5, p. 055806, 2022.

[3] N. Dharmale, R. Mahamune, M. Krishnaiah, and J. K. Kar, "Evaluating the effect of metal, nonmetal, and co-doping on brookite TiO_2," *Nano*, vol. 19, no. 8, p. 2450042, 2024.

[4] F. Giordano *et al.*, "Enhanced electronic properties in mesoporous TiO_2 via lithium doping for high-efficiency perovskite solar cells," *Nature communications*, vol. 7, no. 1, pp. 1–6, 2016.

[5] M. Abd Mutalib *et al.*, "Towards high performance perovskite solar cells: A review of morphological control and htm development," *Applied Materials Today*, vol. 13, pp. 69–82, 2018.

[6] Y.-J. You *et al.*, "Energy recycling under ambient illumination for internet-of-things using metal/ oxide/metal-based colorful organic photovoltaics," *Nanotechnology*, vol. 32, no. 46, p. 465401, 2021.

[7] R. Rani, K. Monga, and S. Chaudhary, "Recent development in electron transport layers for efficient tin-based perovskite solar cells," in *IOP Conference Series: Materials Science and Engineering*, vol. 1258, no. 1, 2022, p. 012015.

[8] Y. Cui, L. Yang, X. Wu, J. Deng, X. Zhang, and J. Zhang, "Recent progress of lead-free bismuth-based perovskite materials for solar cell applications," *Journal of Materials Chemistry C*, vol. 10, no. 44, pp. 16 629–16 656, 2022.

[9] T.-S. Su and T.-C. Wei, "Co-electrodeposition of sn-doped TiO_2 electron-transporting layer for perovskite solar cells," *Physica Status Solidi (a)*, vol. 217, no. 1, p. 1900491, 2020.

[10] X. Liu, Z. Wu, Y. Zhang, and C. Tsamis, "Low temperature zn-doped TiO_2 as electron transport layer for 19% efficient planar perovskite solar cells," *Applied Surface Science*, vol. 471, pp. 28–35, 2019.

[11] M.-C. Wu, T.-H. Lin, S.-H. Chan, Y.-H. Liao, and Y.-H. Chang, "Enhanced photovoltaic performance of perovskite solar cells by tuning alkaline earth metal-doped perovskite-structured absorber and metal doped TiO_2 hole blocking layer," *ACS Applied Energy Materials*, vol. 1, no. 9, pp. 4849–4859, 2018.

[12] X. Yin, Y. Guo, Z. Xue, P. Xu, M. He, and B. Liu, "Performance enhancement of perovskite- sensitized mesoscopic solar cells using nb-doped TiO_2 compact layers," *Nano Research*, vol. 8, pp. 1997–2003, 2015.

[13] Y. Numata, R. Ishikawa, Y. Sanehira, A. Kogo, H. Shirai, and T. Miyasaka, "Nb-doped amorphous titanium oxide compact layer for formamidine-based high efficiency perovskite solar cells by low- temperature fabrication," *Journal of Materials Chemistry A*, vol. 6, no. 20, pp. 9583–9591, 2018.

[14] J. Liu *et al.*, "Restraining Photocurrent Loss of Lead-Free Perovskite Solar Cells by Regulating Surficial Hydroxyl of Fluorine-Doped Tin Oxide," *ACS Applied Energy Materials*, vol. 7, no. 11, pp. 4779–4785, 2024.

[15] N. R. Pochont, Y. R. Sekhar, K. Vasu, and R. Jose, "Nitrogen-doped titanium dioxide as a hole transport layer for high-efficiency formamidine perovskite solar cells," *Molecules*, vol. 27, no. 22, p. 7927, 2022.

[16] R. He, X. Huang, M. Chee, F. Hao, and P. Dong, "Carbon-based solar cells: from single-junction to modules," *Carbon Energy*, vol. 1, no. 1, pp. 109–123, 2019.

[17] S. Arunmetha, N. Dhineshbabu, A. Kumar, and R. Jayavel, "Preparation of sulfur doped TiO_2 nanoparticles from rutile sand and their performance testing in hybrid solar cells," *Journal of Materials Science: Materials in Electronics*, vol. 32, no. 24, pp. 28 382–28 393, 2021.

[18] S. Karthick, S. Velumani, and J. Boucle, "Experimental and SCAPS simulated formamidine perovskite solar cells: A comparison of device performance," *Solar Energy*, vol. 205, pp. 349–357, 2020.

[19] G. Casas, M. ´A. Cappelletti, A. P. Cedola, B. M. Soucase, and E. P. y Blanca, "Analysis of the power conversion efficiency of perovskite solar cells with different materials as hole-transport layer by numerical simulations," *Superlattices and Microstructures*, vol. 107, pp. 136–143, 2017.

[20] Y. Duan *et al.*, "Low-temperature processed tantalum/niobium co-doped TiO_2 electron transport layer for high-performance planar perovskite solar cells," *Nanotechnology*, vol. 32, no. 24, p. 245201, 2021.

[21] A. Kogo, Y. Sanehira, M. Ikegami, and T. Miyasaka, "Brookite TiO_2 as a low-temperature solution-processed mesoporous layer for hybrid perovskite solar cells," *Journal of Materials Chemistry A*, vol. 3, no. 42, pp. 20952–20957, 2015.

[22] A. Kogo, Y. Sanehira, M. Ikegami, and T. Miyasaka, "Anatase and Brookite Electron Collectors from Binder-free Precursor Pastes for Low-temperature Solution-processed Perovskite Solar Cells," *Chemistry Letters*, vol. 45, no. 2, pp. 143–145, 2016.

[23] S. Bhandari, A. Roy, T. K. Mallick, and S. Sundaram, "Morphology modulated brookite TiO_2 and $BaSnO_3$ as alternative electron transport materials for enhanced performance of carbon perovskite solar cells," *Chemical Engineering Journal*, vol. 446, p. 137378, 2022.

[24] Md. Shahiduzzaman *et al.*, "Low-Temperature-Processed Brookite-Based TiO_2 Heterophase Junction Enhances Performance of Planar Perovskite Solar Cells," *Nano Letters*, vol. 19, no. 1, pp. 598–604, 2019.

[25] Q. Guo *et al.*, "Low-temperature processed rare-earth doped brookite TiO_2 scaffold for UV stable, hysteresis-free and high-performance perovskite solar cells," *Nano Energy*, vol. 77, p. 105183, 2020,

[26] Y. Gan *et al.*, "Numerical investigation energy conversion performance of tin-based perovskite solar cells using cell capacitance simulator," *Energies*, vol. 13, no. 22, p. 5907, 2020.

[27] P. Sarkar, S. Tripathy, and K. Baishnab, "Polyvinylpyrrolidone capped electrospun

$CH_3NH_3PbCl_3$ perovskite film as the electron transport layer in perovskite solar cell application," *Solar Energy*, vol. 230, pp. 390–400, 2021.

[28] S. Tao *et al.*, "Absolute energy level positions in tin- and lead-based halide perovskites," *Nature communications*, vol. 10, no. 1, pp. 1–10, 2019.

[29] H.-P. Hsu, L.-C. Li, M. Shellaiah, and K. W. Sun, "Structural, photophysical, and electronic properties of $CH_3NH_3PbCl_3$ single crystals," *Scientific reports*, vol. 9, no. 1, pp. 1–14, 2019.

[30] S. Rai, B. Pandey, and D. Dwivedi, "Modeling of highly efficient and low cost $CH_3NH_3Pb(I_{1-x}Cl_x)_3$ based perovskite solar cell by numerical simulation," *Optical Materials*, vol. 100, p. 109631, 2020.

[31] P. Zhao *et al.*, "Device simulation of inverted $CH_3NH_3PbI_{3-x}Cl_x$ perovskite solar cells based on PCBM electron transport layer and NiO hole transport layer," *Solar Energy*, vol. 169, pp. 11–18, 2018.

[32] H. Wang, Y. Qiang, S. Zheng, P. Wei, and Y. Xie, "Enhanced Efficiency and Stability of Carbon-Based Perovskite Solar Cells by Eva Interface Engineering," *Advanced Materials Interfaces*, vol. 9, no. 10, 2022.

[33] Z. Arshad *et al.*, "Magnesium doped TiO_2 as an efficient electron transport layer in perovskite solar cells,"*Case Studies in Thermal Engineering*, vol. 26, p. 101101, 2021.

[34] M. Abd Mutalib *et al.*, "Performance-Enhancing Sulfur-Doped TiO_2 Photoanodes for Perovskite Solar Cells," *Applied Sciences*, vol. 12, no. 1, p. 429, 2022.

[35] V. Odari, R. Musembi, and J. Mwabora, "Device simulation of sb2s3 solar cells by scaps-1d software," *Africa Journal of Physical Sciences*, vol. 3, pp. 39–54, 2019.

[36] Md. S. Rahman, S. Miah, M. S. W. Marma, and T. Sabrina, "Simulation based Investigation of Inverted Planar Perovskite Solar Cell with All Metal Oxide Inorganic Transport Layers," in *2019 International Conference on Electrical, Computer and Communication Engineering (ECCE)*, IEEE, 2019, pp. 1–6.

[37] Y. M. Lee *et al.*, "Comprehensive Understanding and Controlling the Defect Structures: An Effective Approach for Organic-Inorganic Hybrid Perovskite-Based Solar-Cell Application," *Frontiers in Energy Research*, vol. 6, 2018.

[38] N. K. Noel *et al.*, "Lead-free organic–inorganic tin halide perovskites for photovoltaic applications," *Energy & Environmental Science*, vol. 7, no. 9, pp. 3061–3068, 2014.

[39] L. Ma, F. Hao, C. C. Stoumpos, B. T. Phelan, M. R. Wasielewski, and M. G. Kanatzidis, "Carrier diffusion lengths of over 500 nm in lead-free perovskite $CH_3NH_3SnI_3$ films," *Journal of the American Chemical Society*, vol. 138, no. 44, pp. 14 750–14 755, 2016.

[40] F. Hao, C. C. Stoumpos, D. H. Cao, R. P. Chang, and M. G. Kanatzidis, "Lead-free solid-state organic–inorganic halide perovskite solar cells," *Nature photonics*, vol. 8, no. 6, pp. 489–494, 2014.

[41] F. Hao, C. C. Stoumpos, P. Guo, N. Zhou, T. J. Marks, R. P. Chang, and M. G. Kanatzidis, "Solvent-mediated crystallization of $CH_3NH_3SnI_3$ films for heterojunction depleted perovskite solar cells," *Journal of the American Chemical Society*, vol. 137, no. 35, pp. 11 445–11 452, 2015.

[42] M. Lazemi, S. Asgharizadeh, and S. Bellucci, "A computational approach to interface engineering of lead-free $CH_3NH_3SnI_3$ highly-efficient perovskite solar cells," *Physical Chemistry Chemical Physics*, vol. 20, no. 40, pp. 25 683–25 692, 2018.

[43] H.-J. Du, W.-C. Wang, and J.-Z. Zhu, "Device simulation of lead-free $CH_3NH_3SnI_3$ perovskite solar cells with high efficiency," *Chinese Physics B*, vol. 25, no. 10, p. 108802, 2016.

[44] F. M. Rombach, S. A. Haque, and T. J. Macdonald, "Lessons learned from Spiro-OMeTAD and PTAA in perovskite solar cells," *Energy & Environmental Science*, vol. 14, no. 10, pp. 5161–5190 ,2021.

[45] A. di Paola, M. Bellardita, and L. Palmisano, "Brookite, the Least Known TiO_2 Photocatalyst," *Catalysts*, vol. 3, no. 1, pp. 36–73, 2013.

[46] J. H. Heo *et al.*, "Efficient inorganic–organic hybrid heterojunction solar cells containing perovskite compound and polymeric hole conductors," *Nature photonics*, vol. 7, no. 6, pp. 486–491, 2013.

[47] J.-W. Lee, T.-Y. Lee, P. J. Yoo, M. Grätzel, S. Mhaisalkar, and N.-G. Park, "Rutile TiO_2-based perovskite solar cells," *Journal of Materials Chemistry A*, vol. 2, no. 24, p. 9251, 2014.

[48] B. E. Heredia-Cervera *et al.*, "Anatase, rutile, and brookite TiO_2 electron transport layers for mesoporous carbon-based perovskite solar cells," *APL Energy*, vol. 3, no. 3, 2025.